Electronic structure of single-wall, multiwall, and filled carbon nanotubes

D. Östling, D. Tománek,* and A. Rosén
Department of Physics, Göteborg University and Chalmers University of Technology, S-412 96 Göteborg, Sweden
(Received 6 January 1997)

We determine the electronic structure of single-wall, multiwall, and filled carbon nanotubes using the local-density-functional formalism. In order to handle these extremely inhomogeneous systems of nested graphene cylinders with 10^3–10^4 valence electrons, we adopt a technique that discretizes the eigenvalue problem on a grid and yields simultaneously all occupied and unoccupied states. We apply this formalism to nanotubes, where the ionic background can be described by infinitely thin structureless cylindrical walls, and the electron distribution is subsequently obtained in a self-consistent manner. Comparison with parametrized calculations, which consider explicitly the atomic positions, proves that the essential features of the electronic structure in these systems do not depend on the exact atomic positions. [S0163-1829(97)07220-2]

I. INTRODUCTION

Carbon nanotubes, first discovered as a by-product of carbon fullerene production,[1] have attracted significant attention recently as well-defined, stable, and rigid one-dimensional systems.[2,3] Different aspects of the highly interdisciplinary field of carbon fullerenes and nanotubes have been discussed in a recent book by Dresselhaus, Dresselhaus, and Eklund,[4] and in a recent review by Ebbesen.[5] As in the case of the discovery[6] and bulk production technique[7] for the related C_{60} fullerene molecule, the discovery of nanotubes was very serendipitous. Multiwall nanotubes have been first found in the buildup occurring on the cathode of the carbon arc that is operated in a helium atmosphere to produce fullerenes such as C_{60}. Their outer diameter varies typically between 20 and 200 Å, while the inner diameter is typically of the order of 10–30 Å. The interlayer distance is $\approx$3.4 Å, corresponding to the interlayer distance of graphite. Single-wall nanotubes, on the other hand, have been found to form spontaneously whenever the graphite material used in the arc[8–10] or in laser vaporization[2] was enriched by traces of transition metals such as Co or Ni, acting as a catalyst. Single-wall nanotubes have a much narrower radius distribution, centered around $\approx$12–14 Å.[8–10,2] They grow up to 10^2 μm long, resulting in a high aspect (length over diameter) ratio of up to $\approx 10^5$.

Subsequent to the successful formation of endohedral fullerenes by encapsulating metal atoms in carbon cages,[11] was a synthesis of metal-filled nanotubes. Owing to their low melting point, Pb and Bi were the first elements observed to fill the core of the nanotubes by capillary action.[12,13] Later on, nanotubes filled with Y,[14] Mn,[15] and Gd (Ref. 16) were synthesized, albeit at low yield, directly in the carbon arc. Significant progress resulted from two further technological advances. Tsang *et al.*[17] succeeded in opening nanotubes with nitric acid and filling them with Ni, Co, Fe, and U ions from the solution. Guerret-Piécourt *et al.*[18] synthesized filled tubes directly by adding the respective metal to the electrode material used in the carbon arc. With this technique, in particular the metals Cr and Gd proved to form efficiently long nanowires contained in nanotubes.

Theoretical studies have shown that chirality has a profound effect on the electronic structure of isolated single-wall nanotubes.[19,20] Parametrized calculations addressing only the $pp\pi$ interatomic interactions, which dominate the electronic structure near the Fermi level, indicated that the achiral ''armchair'' (n,n) nanotubes[4] should be metallic, whereas all (n,m) tubes, with $n-m$ a nonzero multiple of 3, should be small-gap semiconductors or semimetals.[19] Nanotubes not fitting in either category should be semiconducting, with a band gap roughly proportional to the reciprocal tube radius.[21] These findings have been found to be qualitatively correct only in tubes with a large diameter, where the $s-p$ hybridization is negligible.[22]

In this study we turn to multiwall and metal filled nanotubes, and discuss how their electronic structure evolves from that of single-wall nanotubes. A self-consistent calculation of the charge distribution in such layered systems turns out to be very difficult, since the determination of eigenstates tends to be either numerically unstable, or fails to reproduce the interlayer states correctly.

Here we present a technique which addresses these problems in systems with cylindrical symmetry. Our approach, which is outlined in Sec. II, is based on a numerical method of Salomonson and Öster,[23] which was originally developed to treat correlation effects in many-body calculations of atoms. We use this technique to treat self-consistently 10^3–10^4 electrons in very inhomogeneous systems such as multiwall and filled nanotubes, as well as nanowires. Results for the charge density, the electrostatic potential, and the electronic density of states of these systems will be presented in Sec. III. Finally, in Sec. IV, we summarize our results.

II. THEORY

In the following we present the formalism to study the electronic structure of single-wall, multiwall, and filled carbon nanotubes as well as nanowires. First, we introduce a very general and numerically stable technique to obtain the complete spectrum of occupied and unoccupied eigenstates of systems with cylindrical symmetry, based on the *ab initio* density-functional formalism. We apply this technique to the above-mentioned systems with extreme spatial variations of the charge density, where we treat the ionic background in an

approximate way. To assess the effect of the exact ionic positions, we use a parametrized linear combination of atomic orbitals technique. In the following, all expressions, unless their dimension is specified, will be given in Hartree atomic units.

A. Density-functional calculation of the complete set of electronic eigenstates of nanotubes

We calculate the electronic structure of nanotubes using the density-functional theory.[24,25] In the electronic ground state, the total energy E is a well-defined functional of the total charge density $\rho(\mathbf{r})$. $E[\rho(\mathbf{r})]$ can then be obtained in a variational manner, with the constraint that the total number of electrons be conserved, by solving self-consistently the set of Kohn-Sham equations[25]

$$[-\tfrac{1}{2}\nabla^2+V_{\rm eff}(\mathbf{r})]\psi_i(\mathbf{r})=\varepsilon_i\ \psi_i(\mathbf{r}),$$

$$\rho(\mathbf{r})=\sum_i^{\rm occ}\ |\psi_i(\mathbf{r})|^2\quad . \tag{1}$$

The effective potential $V_{\rm eff}$ in the local-density-approximation (LDA) formalism is given by

$$V_{\rm eff}(\mathbf{r})=V_{\rm ion}(\mathbf{r})+V_H(\rho(\mathbf{r}))+V_{\rm xc}(\rho(\mathbf{r}))\quad , \tag{2}$$

where $V_{\rm ion}$ is the ionic background potential, V_H is the Hartree potential, and $V_{\rm xc}$ is a local potential describing the effect of exchange and correlation. In the present work, we use the Gunnarsson-Lundqvist parametrization[26] of $V_{\rm xc}$.

The most satisfying approach to determining the electronic states of multiwall nanotubes would be to consider their atomic structure. This could be achieved in a self-consistent manner using the LDA with a linear combination of atomic orbitals (LCAO) basis. However, the large number of carbon atoms needed to describe a long, possibly chiral nanotube makes a simplified approach more attractive. In the following, we focus on the electronic structure arising from the interacting $2s$ and $2p$ valence electrons of carbon, and replace the point charges of the individual C^{4+} ions in the graphitic walls by two-dimensional charged ''sheets'' (''2D jellium background'') of cylindrical symmetry, with uniform surface-charge density σ. For a graphitic honeycomb lattice with a C–C bond length of 2.68 a.u., we obtain $\sigma=+0.428\ e/\text{a.u.}^2$

1. Eigenvalue problem in systems with cylindrical symmetry

The potential due to the ionic background charge of an infinitely long single-wall nanotube of radius R is given by Gauss's law[27] as

$$V_{\rm ion}(r)=\begin{cases}-2\lambda\ \ln(R)+c & \text{for } r\leqslant R\\ -2\lambda\ \ln(r)+c & \text{for } r>R\end{cases}\quad , \tag{3}$$

where $\lambda=2\pi R\sigma$ is the number of electrons per unit length of the nanotube, and c is an arbitrary constant. In multiwall nanotubes the total ionic background potential is a superposition of potentials obtained using Eq. (3) for the individual nanotubes of radius R. Gauss's law gives also a very similar expression for the ionic background potential of an infinitely long, structureless solid wire of radius R,

$$V_{\rm ion}(r)=\begin{cases}-\lambda[(r/R)^2-1]-2\lambda\ \ln(R)+c & \text{for } r\leqslant R\\ -2\lambda\ \ln(r)+c & \text{for } r>R\end{cases}\quad . \tag{4}$$

Here λ is the number of electrons per unit length of the wire, and c is an arbitrary constant. The eigenfunctions of the Kohn-Sham operator for a nanotube or nanowire of length L (with $L\gg R$), aligned with the z axis, can be factorized into radial, azimuthal, and axial parts as

$$\psi_{nmk}(r,\varphi,z)=\frac{1}{\sqrt{\pi L}}R_{nm}(r)e^{im\varphi}\sin\left(\frac{k\pi}{L}z\right)\quad . \tag{5}$$

Here, $n=1,2,3,\ldots$ denotes the radial quantum number, $m=0,\pm1,\pm2,\ldots$ the azimuthal quantum number, and $k=1,2,3,\ldots$ the axial quantum number. The physical significance of $(n-1)$ is the number of radial nodes of ψ_{nmk}. In the corresponding fashion, $|m|$ and $(k-1)$ give the number of azimuthal and longitudinal nodes of ψ_{nmk}, respectively.

We now construct a cylindrical box of large but finite length L, and align the axes of the nanotube and cylinder. The discretization of the spectrum due to the finite length L is minimized for sufficiently large values of L. The most challenging problem is the determination of the radial wave function $R_{nm}(r)$, which we solve by first substituting $R_{nm}(r)=u_{nm}(r)/\sqrt{r}$. The Kohn-Sham Eq. (1) leads to a new equation for $u_{nm}(r)$

$$\left[-\frac{1}{2}\left\{\frac{\partial^2}{\partial r^2}+\frac{1}{4r^2}\right\}+\frac{m^2}{2r^2}+\frac{k^2\pi^2}{2L^2}+V_{\rm eff}(r)\right]u_{nm}(r)=\varepsilon_{nmk}\ u_{nm}(r)\quad . \tag{6}$$

2. Numerically stable technique to solve the eigenvalue problem

A numerical solution of the differential equation (6) for the radial function $u_{nm}(r)$ using a standard point-and-shoot method[28] generally fails if several classically allowed regions are separated by forbidden regions, which is the case in multiwall nanotubes. To solve this differential equation, we adopt a technique by Salomonson and Öster,[23] that was originally developed for atoms, to systems with cylindrical symmetry. The objective is to determine the eigenfunction $u_{nm}(r)$ on a linear grid of N points $r_1,\ldots,r_N$, separated by a constant distance h, inside the cylindrical box. To evaluate the kinetic term in the radial Eq. (6), we use the symmetric five-point formula for the second-order derivative of a function $u_{nm}(r)$,

$$\frac{\partial^2u(r)}{\partial r^2}=\frac{1}{12h^2}[-u(r-2h)+16u(r-h)-30u(r)+16u(r+h)-u(r+2h)]+O(h^4)\quad . \tag{7}$$

Substituting expression (7) into Eq. (6) leads to a set of N coupled linear equations for $u_{nm}(r_i)$ that can be formulated as an eigenvalue problem

$$(A+D)\mathbf{u}_{nm}=\varepsilon\mathbf{u}_{nm}\quad . \tag{8}$$

Determining the eigenvector $\mathbf{u}=[u_{nm}(r_1),u_{nm}(r_2),\ldots,u_{nm}(r_N)]$ in Eq. (8) is equivalent to solving Eq. (6) on the radial grid. The matrix describing the operator A is diagonal, with its elements given by

$$A_{ii}=\frac{m^2}{2r_i^2}+\frac{k^2\pi^2}{2L^2}+V_{\rm ion}(r_i)+V_H(r_i)+V_{\rm xc}(r_i), \tag{9}$$

where $i=1,2,\ldots,N$. D is the symmetric band matrix obtained from Eq. (7), given by

$$D=-\frac{1}{24h^2}\begin{pmatrix} -30+\frac{1}{4r_1^2} & 16 & -1 & 0 & 0 & \cdots & 0 \\ 16 & -30+\frac{1}{4r_2^2} & 16 & -1 & 0 & \cdots & 0 \\ -1 & 16 & -30+\frac{1}{4r_3^2} & 16 & -1 & \cdots & -1 \\ \vdots & \vdots & \vdots & \vdots & \vdots & \ddots & 16 \\ 0 & 0 & 0 & 0 & -1 & 16 & -30+\frac{1}{4r_N^2} \end{pmatrix}. \tag{10}$$

We require $A+D$ to be symmetric in order to obtain a real eigenvalue ε in Eq. (8) and a radial eigenfunction $u_{nm}(r)$ that is real and doubly differentiable everywhere inside the cylinder. The above form of D implies that the wave functions vanish outside the grid, i.e., all electrons are contained in the cylindrical box. The asymptotic behavior of $u_{nm}(r)$ in the region close to the z axis, $u_{nm}(r)\propto r^{|m|+1/2}$, has to be enforced, while still keeping the matrix D symmetric.[23] To achieve this, we focus on the matrix elements D_{11}, D_{12}, D_{21}, and D_{22}. The $A+D$ matrix can be symmetrized by extending the radial axis to the left of the first grid point, and using the ansatz

$$u_{nm}(r_0)=\alpha\left[\frac{u_{nm}(r_0)}{u_{nm}(r_1)}\right]u_{nm}(r_1)+(1-\alpha)\left[\frac{u_{nm}(r_0)}{u_{nm}(r_2)}\right]u_{nm}(r_2),$$

$$u_{nm}(r_{-1})=\left[\frac{u_{nm}(r_{-1})}{u_{nm}(r_1)}\right]u_{nm}(r_1) \tag{11}$$

for the function values at the new grid points r_{-1} and r_0 preceding the first grid point r_1. The function value ratios occurring in Eq. (11) are determined using the appropriate asymptotic behavior of $u_{nm}(r)$. The free parameter α is then chosen in such a way that $D_{12}=D_{21}$.

The last difficulty in the solution of the eigenvalue Eq. (6) occurs due to the divergence of two terms in the differential operator at $r=0$. We address this problem in systems with nonzero charge density near the cylinder axis by introducing a very fine grid near $r=0$, and displacing this grid laterally by a small distance, e.g., $0.1h$. In this case, none of the microgrid points $r_{-1}=0.1h$, $r_0=1.1h$, $r_1=2.1h$, ... coincides with $r=0$. Interpolation is then used to determine the radial wave function and all its derivatives even in the region close to the cylinder axis.

We note that the total number of eigenstates is determined by the rank N of the matrices A and D in Eq. (8) (that is related to the radial grid) and not the total number of electrons. Consequently, this approach can be used to determine also the unoccupied states, which are the basis of calculations determining the collective response of these systems, e.g., using the time-dependent LDA (TDLDA) or the LDA-based random phase-approximation technique.

B. Parametrized linear combination of atomic orbitals (LCAO) technique

To investigate the effect of discrete atomic positions on the electronic structure of nanotubes, we made use of the parametrized linear combination of atomic orbitals technique, since the full LDA theory is too demanding on computer resources. It has been shown that mapping LDA results for characteristic structures onto parameters of a LCAO Hamiltonian provides a very useful and efficient way to determine the electronic states of carbon systems.[29] The nearest-neighbor LCAO Hamiltonian we use reads

$$H_{\rm LCAO}=\sum_i\sum_\beta \epsilon^0_{i\beta}a^\dagger_{i\beta}a_{i\beta} + \sum_{i<j}\sum_{\beta,\beta'} t_{i\beta,j\beta'}(a^\dagger_{i\beta}a_{j\beta'}+\text{c.c.}) \quad . \tag{12}$$

In our notation, β and β' refer to electronic levels of the cluster and isolated atoms, respectively, and Roman indices denote atomic sites. In the LCAO calculations of carbon nanotubes, we use four orbitals of s, p_x, p_y, and p_z characters on each atomic site, and Slater-Koster parameters[29] for the matrix elements of the Hamiltonian (12).

III. RESULTS

In Fig. 1 we present results for the charge distribution and the total potential of a hollow single-wall nanotube, a thin nanowire, a tube filled by a nanowire, and a double-wall nanotube. In these calculations, the C^{4+} ion charges in each nanotube wall have been smeared out into infinitely thin cylindrical walls, representing a 2D jellium background, and

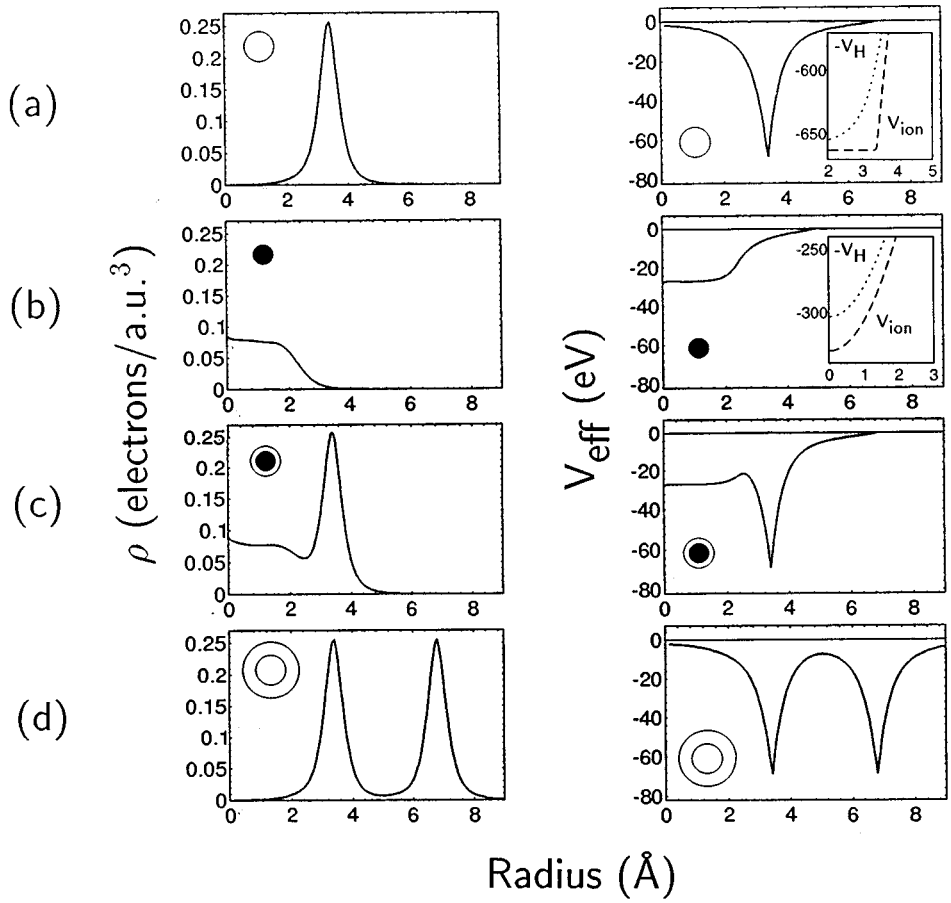

FIG. 1. Results for the self-consistent radial charge density $\rho(r)$ and effective total potential $V_{\text{eff}}(r)$ of (a) a hollow single-wall carbon nanotube with radius $R=3.4$ Å, (b) a solid Pb nanowire with $R=2.4$ Å, (c) the nanowire (b) encapsulated in the nanotube (a), and finally (d) a double-wall nanotube, consisting of the nanotube (a) enclosed inside a nanotube with the radius $R=6.8$ Å. The ionic and electronic contributions to V_{eff} are shown as insets in subfigures (a) and (b). Symbols are introduced to distinguish the different systems in the subfigures.

only the C $2s$ and C $2p$ valence electrons have been considered as active. Our description of Pb nanowires within the jellium model follows Ref. 30. We use $r_s=2.30$ a.u. for the Wigner-Seitz radius, and a valence $Z=4$ for Pb in the ground-state configuration $[\text{Xe}]4f^{14}5d^{10}6s^26p^2$. The jellium background charge density of Bi, which has also been found to fill carbon nanotubes, is only $\approx 25\%$ higher than in Pb. Consequently, we expect qualitatively similar results for nanowires of these two elements.

It is instructive to discuss the behavior of $V_{\text{eff}}=V_{\text{ion}}+V_{\text{el}}$ in terms of its ionic and electronic components V_{ion} and V_{el}, where $V_{\text{el}}=V_H+V_{\text{xc}}$. Since the systems we consider are charge neutral, we find V_{el} to show generally the same behavior as $-V_{\text{ion}}$ throughout the space, causing V_{eff} to vanish in the vacuum region inside or outside the nanostructures, shown in the insets of Figs. 1(a) and 1(b).

As mentioned in Sec. II, the electronic states in systems with cylindrical symmetry are characterized by the quantum numbers n, m, and k, where $(n-1)$ corresponds to the number of radial nodes, $|m|$ corresponds to the number of azimuthal nodes, and $(k-1)$ is the number of longitudinal nodes of the wave function. In order to understand the nature of such wave functions in cylindrical symmetry better, we first turn to analogous spherical systems, such as the C_{60} fullerene, that have been studied extensively from this point of view.

The C_{60} molecule with icosahedral symmetry contains all 60 atoms in equivalent sites on a hollow, spherical graphitic shell. The near-spherical structure of C_{60} suggests representing the wave functions in a spherical basis.[31] Indeed, results of self-consistent LDA calculations for C_{60} suggest that to a good approximation, occupied eigenstates of C_{60} can be characterized by radial and angular quantum numbers.[32] The description of C_{60} by a spherically symmetric hollow cage turned out to be a very reasonable first approximation.[33,34] An adequate description of further level splitting due to symmetry reduction can be achieved using perturbation theory. This approach has been used successfully to describe the (rather small) effect in C_{60} introduced by the reduction from spherical to icosahedral symmetry.[33] Since atomic positions are ignored in the spherical hollow cage description of C_{60}, there is no direct way to distinguish the electronic states associated with individual interatomic σ and π bonds. The distinction between the σ and π *states* is rather based on the fact that the graphitic layer is a nodal layer for the nonbonding $pp\pi$ molecular orbitals, whereas it is not a nodal layer for the σ orbitals. Correspondingly, σ states can be associated with wave functions that have no radial nodes, whereas

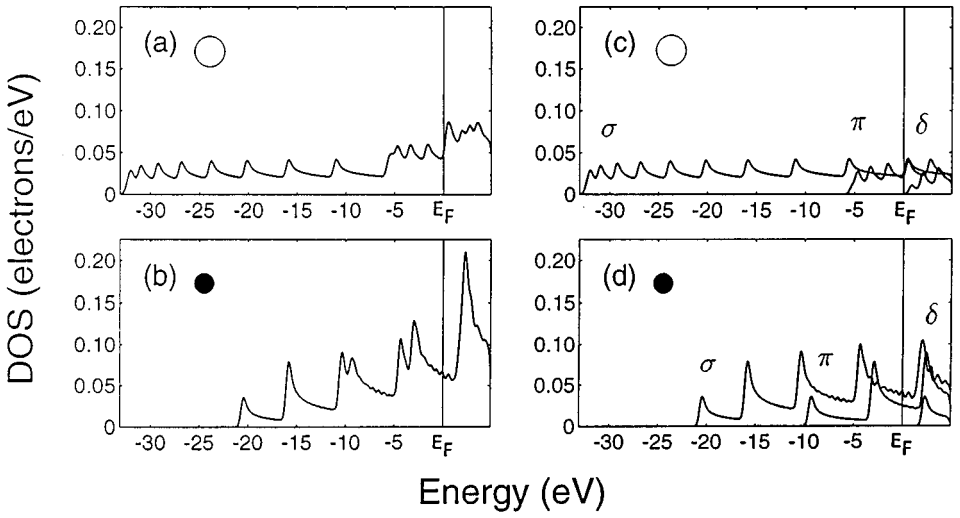

FIG. 2. Total electronic density of states (DOS) of (a) a hollow single-wall nanotube with the radius $R=3.4$ Å, and (b) a solid Pb nanowire with $R=2.4$ Å, with E_F at energy zero. (c) The partial DOS with respect to the radial quantum number n of the nanotube (a) shows the $n=1$ (σ), $n=2$ (π), and $n=3$ (δ) bands extending above -33 eV, -5 eV, and E_F, respectively. (d) The corresponding partial DOS of the nanowire (b) shows the σ, π, and δ bands extending above -21, -10, and $+2$ eV, respectively. Symbols are introduced to distinguish the different systems in the subfigures.

π states have a single node in the radial wave function. The angular arrangement of the wave function nodes is given by the spherical harmonics and the angular quantum number $l=0,1,2,\ldots$. An analysis of the occupied levels of the C_{60} molecule shows that the levels close to the highest occupied molecular orbital are of π type, whereas the more deeply bound states are of σ type.[35]

Since the interatomic bonding in the nanotubes and the C_{60} fullerene are very similar, we expect that a description of the C^{4+} ions by a homogeneously charged, infinitely thin layer will also provide a valid description for the nanotube. As in the C_{60} molecule, we will distinguish σ states with no radial node from π states with one radial node in the graphene wall. This is illustrated in Fig. 2, which displays the total and partial electronic densities of states (DOS) for the isolated nanotube and the nanowire discussed above and in Fig. 1.

The comparison between the total DOS for the isolated nanotube in Fig. 2(a) and its decomposition into partial DOS according to the radial wave number n in Fig. 2(c) shows an energy-level spectrum starting 33 eV below the Fermi level with states containing no radial nodes, establishing that bonding originates from the σ states. The π states are much higher in energy and closer to the Fermi level, establishing their essentially nonbonding character. None of the $n=3$ (δ) band states is occupied in the ground state, but such states are important when studying electronic excitations. Similarly, our results for the total and partial DOS of the Pb nanowire, shown in Figs. 2(b) and 2(d), suggest that only $n=1$ (σ) and $n=2$ (π) states are occupied in this system.

Both the nanotube and the nanowire show substructure in the DOS of each n-decomposed subband, that is associated with the azimuthal quantum number m and the longitudinal momentum k. The peaks in the partial densities of states are van Hove singularities that occur in one-dimensional systems.[30] Each of these singularities is associated with a particular azimuthal quantum number $|m|$; singularities occurring at higher energies are associated with larger values of $|m|$. We will refer back to Fig. 2 in the following, when discussing the DOS of more complex systems, such as multiwall and filled nanotubes.

A metal filled nanotube can be viewed as an extremely thin nanowire that is protected from oxidation by an external graphitic shell. This system is a near-ideal realization of a one-dimensional conductor that can be studied quantitatively with our model description of nanowires and nanotubes. We will use our 2D jellium background approach to investigate the evolution of the ground-state electronic structure of nanotubes due to their filling by a metal, or with increasing number of cylindrical graphitic walls. In Fig. 3 we compare the DOS of a Pb-filled single-wall nanotube to that of a double-wall nanotube. The former consists of a Pb nanowire with the radius of 2.4 Å inside a nanotube with a radius of 3.4 Å. The total and partial DOS of this encapsulated nanowire is shown in Figs. 3(a) and 3(c), respectively. The double-wall nanotube consists of a 3.4-Å radius tube nested inside a 6.8-Å radius nanotube. The total and partial DOS of this system is presented in Figs. 3(b) and 3(d), respectively. Note that the vertical axes in Figs. 3(c) and 3(d), depicting the partial DOS, have been expanded by a factor of 4 to display the many subbands better.

The occupied bandwidth of the double-wall nanotube, shown in Fig. 3(b), is very similar to that of the single-wall nanotube of Fig. 2(a). As in the single-wall tube, with results shown in Fig. 2(c), we can distinguish between occupied σ and π bands in the partial densities of states of the double-wall nanotube, depicted in Fig. 3(d). This result looks plausible since, with an increasing number of walls, we expect an evolution of the electronic density of states toward that of graphite which also shows occupied π and σ bands.

The total and partial densities of states of the filled nanotube, shown in Figs. 3(a) and 3(c), provide insight into the electronic structure of this system that has not been investigated theoretically so far, to our knowledge. Comparison

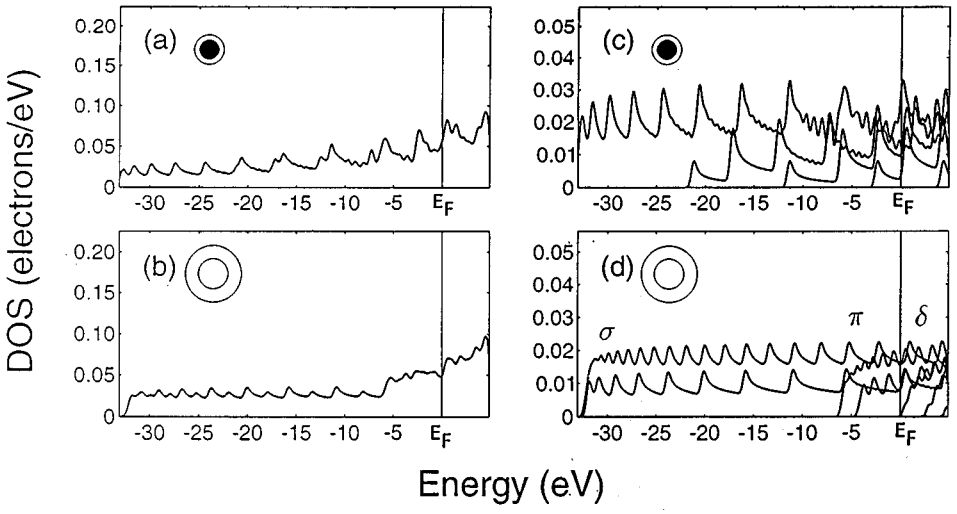

FIG. 3. (a) Total electronic density of states (DOS) of an encapsulated nanowire, for a geometry defined in Fig. 1(c), to be compared to the DOS of its isolated components, given in Figs. 2(a) and 2(b). (b) Total DOS of the double-wall nanotube, defined in Fig. 1(d). (c) Decomposition of the DOS in (a) into its components according to the radial quantum number n, for $n=1,\ldots,5$. (d) Decomposition of the DOS in (b) into its components according to the radial quantum number n, for $n=1,\ldots,7$. The DOS scale in (c) and (d) has been expanded for better viewing. Symbols are introduced to distinguish the different systems in the subfigures.

with the results for an isolated tube in Fig. 2(c) and the nanowire in Fig. 2(d) indicates that the nanowire states hybridize strongly with the π band of the surrounding nanotube in the composite system. The DOS of the encapsulated nanowire in Fig. 3(a) appears to be more irregular near E_F than that of the double-wall nanotube in Fig. 3(b). The comparison between the partial DOS of the encapsulated nanowire in Fig. 3(c) and the partial DOS of the isolated nanotube in Fig. 2(c) and the isolated nanowire in Fig. 2(d) indicates that the density of states of the encapsulated wire is dominated by the nanowire states at the Fermi level.

So far, our discussion of the electronic structure of nanotubes has been based on the assumption that the point charges of the C^{4+} ion cores in the graphene sheets are smeared out into two-dimensional layers. Ignoring the honeycomb structure of carbon atoms in the tubules is certainly a serious simplification that needs to be justified. In the following we will compare our results for a single-wall 2D jellium background nanotube to those based on a parametrized four-state (s,p_x,p_y,p_z) LCAO Hamiltonian[29] which does consider the atomic positions explicitly.

Recent experimental and theoretical evidence indicates that achiral ''armchair'' nanotubes prevail among the catalytically grown single-wall tubes.[2] Consequently, in Fig. 4 we compare in our results for a 2D jellium background single-wall nanotube with those for a (5,5) armchair nanotube[4] with a discrete graphitic structure and the same radius $R=3.4$ Å. The lattice on the cylinder wall is periodic, with a 2.5-Å-high cylindrical unit cell containing 20 atoms. The LCAO band structure along the Γ-X direction in the Brillouin zone is displayed in Fig. 4(a). The corresponding density of states, shown in Fig. 4(b), is to be compared to the DOS based on the 2D jellium background model, which is reproduced in Fig. 4(c) from Fig. 2(a).

Before attempting a more detailed comparison between the densities of states of the discrete and 2D jellium background tubes, we must realize that the DOS depends strongly on the tube chirality.[19,20] The absence of atomic structure in the 2D jellium background tubes is in some sense equivalent to averaging over all chiral angles. We will limit our following discussion to more global properties, such as the structure and the width of the occupied bands, the hybridization, and the character of states in specific energy regions.

The band structure of the (5,5) armchair nanotube in Fig. 4(a) is symmetric about the Fermi level close to E_F. The nonzero density of states at E_F in Figs. 4(b) and 4(c) suggests this nanotube to be metallic, in agreement with previous results.[19,20] The band structure in Fig. 4(a) shows a grouping of states at the X point near $E=-2.5$ eV, which spread to a ≈ 6 eV wide band below the Fermi level. An examination of their character revealed that all these states originate from a $pp\pi$ interaction and have a radial node. The character and width of this subband is in excellent agreement with that of the occupied π band in the 2D jellium background model of the nanotube in Figs. 4(a) and 2(c). It is gratifying to obtain such a good agreement for states close to the Fermi level which determine the dielectric and optical properties of these systems.

A separate band in the range -20 eV$<E<-6$ eV evolves from levels that group near -17.5 eV$<E<-11.0$ eV at the X point. These states originate from interatomic $ss\sigma$, $sp\sigma$, $pp\sigma$, and $pp\pi$ interactions, and have *no* radial nodes. The character of these states is the same as that of the σ band in the 2D jellium background tube model in Figs. 4(a) and 2(c). Comparison between Figs. 4(b) and 4(c), however, shows that the σ bandwidth of the 2D jellium background tube is ≈ 10 eV larger than that of the discrete tube, based on the LCAO calculation. This large difference can be traced back to the significantly larger degree of electron delocalization, once the C^{4+} ions are smeared out to a continuous positive background.

The van Hove singularities, which are typical of one-dimensional systems and dominate the density of states of

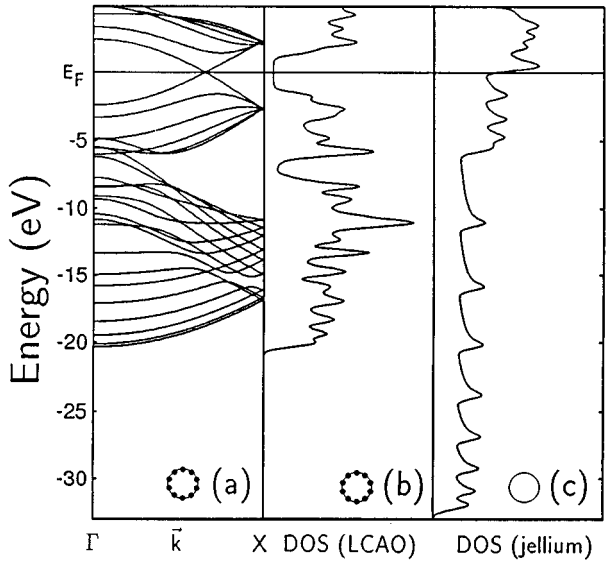

FIG. 4. (a) Band structure $\varepsilon(\mathbf{k})$ and (b) the total electronic density of states (DOS) of a (5,5) ''armchair'' nanotube with the radius $R=3.4$ Å and discrete atomic positions, calculated using the parametrized linear combination of atomic orbitals (LCAO) formalism of Ref. 29. (c) Results of Fig. 2(a) for the DOS of a hollow structureless single-wall nanotube with the radius $R=3.4$ Å are reproduced for the sake of simple comparison. Symbols are introduced to distinguish the different systems in the subfigures.

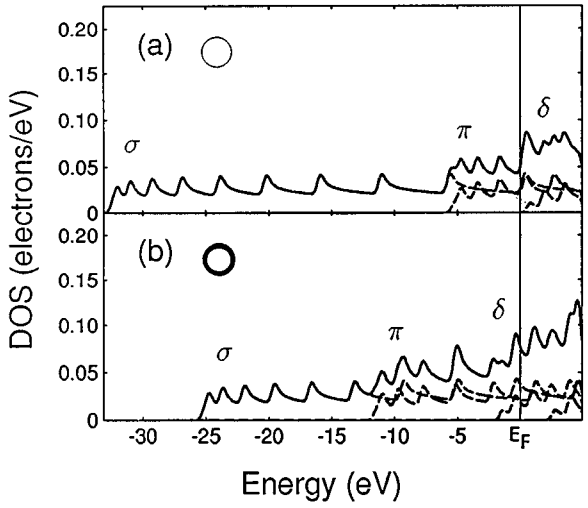

FIG. 5. Total density of states (solid line) and its decomposition into components according to the radial quantum number n (dashed lines) for a hollow single-wall nanotube of radius $R=3.4$ Å. (a) Results of Fig. 2(a) for a nanotube with an infinitely thin structureless wall are compared in (b) to results based on the approach of Ref. 34 that describe the graphitic wall by a hollow cylinder of thickness $d=1.75$ Å, consisting of jellium with a free-electron sphere radius $r_s=1.23$ a.u. Symbols are introduced to distinguish the different systems in the subfigures.

the 2D jellium background nanotube in Fig. 4(c), are also present in the LCAO results in Fig. 4(b), especially near the lower end of the σ band. This means that the parametrized LCAO technique reflects correctly the one-dimensional axial as well as the radial and azimuthal states. We conclude that both techniques yield electronic spectra that can be characterized by the radial, azimuthal, and axial quantum numbers n, m, and k, with consistent level ordering.

Finally, we investigated the degree to which our results would be affected if the C^{4+} ions were smeared out into a continuous jellium background of finite (instead of zero) thickness. Such an approach had been used previously to describe the electronic structure of C_{60}.[34] For the sake of comparison, we reproduced the density of states of our 2D jellium background nanotube of Fig. 2(a) in Fig. 5(a), and compared it to the DOS for the corresponding thick jellium background nanotube in Fig. 5(b). We used the Wigner-Seitz radius $r_s=1.23$ a.u. of Ref. 34, that had been calibrated for C_{60}, and obtained a thickness of $d=1.75$ Å for the hollow cylinder describing the jellium background. The total densities of states for both systems are given by the solid lines, and the partial DOS corresponding to $n=1,2,3$, and 4 by the dashed lines in Figs. 5(a) and(b).

Introducing the ionic background of a thick cylindrical wall leads to a shallower self-consistent potential than in the case of the infinitely thin wall, shown in Fig. 1(a). This would cause an upward shift of the electronic levels, and increase the degree of electron delocalization, thus affecting the occupied bandwidth with respect to the 2D jellium background. To improve agreement with results of full-scale LDA, stabilized jellium[36] has been used instead of ''regular'' jellium to perform thick jellium background calculations of C_{60}.[34] The stabilized jellium model[36] had been introduced as a way to correct negative surface energies in systems with high electron density (or small r_s values), by adding a negative structureless pseudopotential to the ionic potential. The lowering of the ionic potential especially inside the jellium, where r_s is small, leads to a reduction of the electron spill-out beyond the jellium edge. We did not consider this structureless pseudopotential in our calculations for an infinitely long tube in Fig. 5(b), since for this system the divergence of the background potential $V_{\text{ion}}(r)\propto\ln(r)$ for $r\to\infty$ is no longer counterbalanced by the corresponding electronic potential in presence of the new pseudopotential.

A comparison between our results in Figs. 5(a) and 5(b) suggests that introducing a finite-width ionic background results in a contraction of the σ band, a factor-of-2 expansion of the π band, and partial occupation of the δ band associated with $n=3$. The relative stabilization of π and δ states with respect to the bottom of the σ band in thick jellium is a simple consequence of the stronger binding energy dependence of states with radial nodes on the radial width of the attractive region. Consequently, graphitic jellium thickness can be used as a parameter to adjust the widths and relative positions of these bands. Another possibility to improve the agreement between jellium calculations and more realistic *ab initio* results would be to introduce nonlocal corrections to the potential that would depend on the quantum numbers of the state, in the spirit of nonlocal Hamann-Schlüter-Chiang pseudopotentials.[37]

We conclude that the parameter-free 2D jellium background model is superior to the thick jellium background model, especially when describing the occupied electronic states near the Fermi level. For relatively small systems, such as narrow single-wall nanotubes, the best way to obtain more

realistic results would be to perform a self-consistent density-functional calculation for a realistic nanotube containing electrons in a discrete lattice of C^{4+} ions rather than a near structureless positive continuum. For more complex systems containing multiple layers, the introduction of a 2D jellium background model and our technique to determine the entire electronic spectrum by straightforward diagonalization appears to be the most viable alternative.

IV. SUMMARY

We have used the *ab initio* local-density-functional formalism to study the electronic structure of a single-wall carbon nanotube, a Pb nanowire, a nanotube ''filled'' by a Pb nanowire, and a double-wall nanotube. We describe nested carbon nanotubes by smearing the C^{4+} ion charges into 2D jellium background cylinders representing the graphene layers and treating the active C $2s$ and C $2p$ electrons self-consistently. In order to handle the extremely inhomogeneous system of multiwall tubes with 10^3–10^4 electrons, we have developed a formalism that discretizes the eigenvalue problem on a grid and yields a *complete* set of occupied and unoccupied states. The self-consistent electronic structure of infinitely long nanotubes represented by the 2D jellium background model compares favorably with parametrized LCAO calculations that take atomic structure into account. The electronic spectra of single-wall, multiwall, and filled nanotubes, as well as nanowires, can be characterized by the radial, azimuthal and axial quantum numbers n, m, and k. These quantum numbers are reflected in our results based on the self-consistent 2D jellium background model and the parametrized LCAO technique that considers the atomic structure.

ACKNOWLEDGMENTS

We would like to thank P. G. Reinhard, Sten Salomonson, Håkan Warston, Seong Gon Kim, and Henrik Grönbeck for many stimulating and encouraging discussions. The authors acknowledge financial support from the Swedish Natural Science Research Council, NFR (Contract No. F-FU 02560-335), and funding by NFR and the National Swedish Board for Technical Development, NUTEK, through the Interdisciplinary Materials Research Consortium ''Clusters and Ultrafine Particles.'' One of us (D.T.) acknowledges partial financial support by the National Science Foundation under Grant No. PHY-92-24745 and the Office of Naval Research under Grant No. N00014-90-J-1396, and the hospitality of the Department of Physics at Chalmers University.

*Permanent address: Department of Physics and Astronomy, Michigan State University, East Lansing, Michigan 48824–1116.

[1] S. Iijima, Nature **354**, 56 (1991).
[2] A. Thess, R. Lee, P. Nikolaev, H. Dai, P. Petit, J. Robert, C. Xu, Y. H. Lee, S. G. Kim, D. T. Colbert, G. Scuseria, D. Tománek, J. E. Fischer, and R. E. Smalley, Science **273**, 483 (1996).
[3] M. M. J. Treacy, T. W. Ebbesen, and J. M. Gibson, Nature **381**, 678 (1996).
[4] M. S. Dresselhaus, G. Dresselhaus, and P. C. Eklund, *Science of Fullerenes and Carbon Nanotubes* (Academic, San Diego, 1996).
[5] T. W. Ebbesen, Phys. Today **49** (6), 26 (1996).
[6] H. W. Kroto, J. R. Heath, S. C. O'Brien, and R. F. Curl, Nature **318**, 162 (1985).
[7] W. Krätschmer, L. D. Lamb, K. Fostiropoulos, and D. R. Huffman, Nature **347**, 354 (1990).
[8] S. Iijima and T. Ichihashi, Nature **363**, 603 (1993).
[9] D. S. Bethune, C. H. Kiang, M. S. de Vries, G. Gorman, R. Savoy, J. Vazquez, and R. Beyers, Nature **363**, 605 (1993).
[10] P. M. Ajayan *et al.*, Chem. Phys. Lett. **215**, 509 (1993).
[11] D. S. Bethune, R. D. Johnson, J. R. Salem, M. S. de Vries, and C. S. Yannoni, Nature **366**, 123 (1993).
[12] P. M. Ajayan and S. Iijima, Nature **361**, 333 (1993).
[13] P. M. Ajayan, T. W. Ebbesen, T. Ichihashi, S. Iijima, K. Tanigaki, and H. Hiura, Nature **362**, 522 (1993).
[14] S. Seraphin, D. Zhou, J. Jiao, J. C. Withers and R. Loutfy, Nature **362**, 503 (1993).
[15] P. M. Ajayan, C. Colliex, J. M. Lambert, P. Bernier, L. Barbedette, M. Tencé, and O. Stephan, Phys. Rev. Lett. **72**, 1722 (1994).
[16] S. Subramoney, R. S. Ruoff, D. C. Lorents, B. Chan, R. Malhotra, M. J. Dyer, and K. Parvin, Carbon **32**, 507 (1994).
[17] S. C. Tsang, Y. K. Chen, P. J. F. Harris, and M. L. H. Green, Nature **372**, 159 (1994).
[18] C. Guerret-Piécourt, Y. Le Bouar, A. Loiseau, and H. Pascard, Nature **372**, 761 (1994).
[19] R. Saito, M. Fujita, G. Dresselhaus, and M. S. Dresselhaus, Appl. Phys. Lett. **60**, 2204 (1992).
[20] N. Hamada, S. Sawada, and A. Oshiyama, Phys. Rev. Lett. **68**, 1579 (1992).
[21] J. W. Mintmire, D. H. Robertson, B. I. Dunlap, R. C. Mowrey, D. W. Brenner, and C. T. White, in *Electrical, Optical, and Magnetic Properties of Organic Solid State Materials*, edited by L. Y. Chiang, A. F. Garito, and D. J. Sandman, MRS Symposia Proceedings No. 247 (Materials Research Society, Pittsburgh, 1992), p. 339.
[22] X. Blase, L. X. Benedict, E. L. Shirley, and S. G. Louie, Phys. Rev. Lett. **72**, 1878 (1994).
[23] S. Salomonson and P. Öster, Phys. Rev. A **40**, 5559 (1989).
[24] P. Hohenberg and W. Kohn, Phys. Rev. B **136**, 864 (1964).
[25] W. Kohn and L. J. Sham, Phys. Rev. A **140**, 1133 (1965).
[26] O. Gunnarsson and B. I. Lundqvist, Phys. Rev. B **13**, 4274 (1976).
[27] J.D. Jackson, *Classical Electrodynamics*, 2nd ed. (Wiley, New York, 1975).
[28] S. E. Koonin, *Computational Physics* (Benjamin/Cummings, Menlo Park, CA, 1986).
[29] D. Tománek and M. A. Schluter, Phys. Rev. Lett. **67**, 2331 (1991).
[30] N. W. Ashcroft and N. D. Mermin, *Solid State Physics* (Saunders College Publishing, Philadelphia, 1976).
[31] M. Braga, S. Larsson, A. Rosén, and A. Volosov, Astron. Astrophys. **245**, 232 (1991).
[32] J. L. Martins, N. Troullier, and J. H. Weaver, Chem. Phys. Lett. **180**, 457 (1991).
[33] K. Yabana and G. F. Bertsch, Phys. Scr. **48**, 633 (1993).

[34] C. Yannouleas and U. Landman, Chem. Phys. Lett. **217**, 175 (1994).
[35] E. Westin and A. Rosén, Int. J. Mod. Phys. B **6**, 3893 (1992).
[36] J. P. Perdew, H. Q. Tran, and E. D. Smith, Phys. Rev. B **42**, 11 627 (1990).
[37] D. R. Hamann, M. Schluter, and C. Chiang, Phys. Rev. Lett. **43**, 1494 (1979).